

This is the peer reviewed version of the following article:

Role of cerium oxide in bioactive glasses during catalytic dissociation of hydrogen peroxide / Benedetti, Francesco; Amidani, Lucia; Pelli Cresi, Jacopo Stefano; Boscherini, Federico; Valeri, Sergio; D'Addato, Sergio; Nicolini, Valentina; Malavasi, Gianluca; Luches, Paola. - In: PHYSICAL CHEMISTRY CHEMICAL PHYSICS. - ISSN 1463-9076. - 20:36(2018), pp. 23507-23514-23514. [10.1039/c8cp02271b]

*Terms of use:*

The terms and conditions for the reuse of this version of the manuscript are specified in the publishing policy. For all terms of use and more information see the publisher's website.

23/09/2024 18:41

(Article begins on next page)



## Role of cerium oxide in bioactive glasses during catalytic dissociation of hydrogen peroxide

Francesco Benedetti<sup>a,b</sup>, Lucia Amidani<sup>c</sup>, Jacopo Stefano Pelli Cresi<sup>a,b</sup>, Federico Boscherini<sup>d,e</sup>, Sergio Valeri<sup>a,b</sup>, Sergio D'Addato<sup>a,b</sup>, Valentina Nicolini<sup>f</sup>, Gianluca Malavasi<sup>f</sup> and Paola Luches<sup>\*b</sup>

Received 00th January 20xx,  
Accepted 00th January 20xx

DOI: 10.1039/x0xx00000x

[www.rsc.org/](http://www.rsc.org/)

The addition of cerium oxide to bioactive glasses, important materials for bone tissue regeneration, has been shown to induce multifunctionality, combining a significant bioactivity with antioxidant properties. We provide a real time investigation of the evolution of the electronic properties of highly diluted cerium ions in a liquid environment containing hydrogen peroxide - the most abundant reactive oxygen species in living cells. This challenging task is undertaken by means of high-energy resolution fluorescence detected x-ray absorption near-edge spectroscopy at the Ce L<sub>3</sub> edge. We investigate samples with variable compositions and different morphologies. We relate the observed spectroscopic modifications not only to variations in the concentration of the two Ce oxidation states in the samples, but also to changes in the local atomic environment of Ce ions, providing a clear picture of the role of cerium ions in the dissociation of hydrogen peroxide. The obtained results contribute to the understanding of the mechanisms which come into play in the process and provide a basis for the optimization of the functionalities of this class of materials.

### Introduction

Hydrogen peroxide (H<sub>2</sub>O<sub>2</sub>) is one of the most abundant reactive oxygen species (ROS) in living cells, and it is responsible for oxidative damage<sup>1</sup>. In our body the catalase enzyme is effective in preventing the harmful effect of H<sub>2</sub>O<sub>2</sub>. However, in several circumstances an imbalance between ROS and enzymes can occur, causing a number of diseases<sup>2-4</sup>. Reducible oxides, and cerium oxide in particular, in the form of nanoparticles have shown to have a relevant radical scavenging activity, ascribed to the possibility for the cations to reversibly switch between two oxidation states<sup>5-7</sup>. The introduction of an antioxidant functionality is particularly important for biomaterials, which are implanted in the human body by surgery to replace or repair damaged tissues. The inflammation which often follows increases the generation of ROS, and it induces a situation of oxidative stress. This imbalance propagates the inflammation, which may need a long time to achieve a complete recovery<sup>8</sup>. In this scenario,

reducible oxides, such as cerium oxide, which are effective in the conversion of ROS to non-dangerous species, represent good candidates as additives for biomaterials, to confer additional enzyme-like antioxidant properties. In previous papers we have shown that the inclusion of small concentrations of cerium oxide within bioactive glasses, developed for bone implants<sup>9,10</sup>, promotes a very efficient dissociation of H<sub>2</sub>O<sub>2</sub>, i.e. a catalase mimetic activity<sup>11-13</sup>, as well as a superoxide-dismutase mimetic activity<sup>13</sup>. However, the glass bioactivity, i.e. the ability to induce the formation of bone tissue on its surface, was shown to decrease with increasing cerium oxide concentration<sup>12,13</sup>. Moreover, a stabilizing effect of phosphorous on Ce ions in the 3+ oxidation state has been hypothesized, based on the different enzyme mimetic activities of glasses with and without phosphorous in their composition<sup>12</sup>. Glasses with a slightly different composition and a mesoporous morphology have recently shown to have a higher catalase mimetic activity, as well as a higher bioactivity compared to molten glasses, and they represent an important step towards the optimization of the material multi-functionalities<sup>14</sup>. A relevant aspect towards a rational achievement of this goal is the understanding of the atomic scale mechanisms which occur when H<sub>2</sub>O<sub>2</sub> is dissociated. The modifications which come into play in the material during its activity have often been studied ex-situ after soaking in H<sub>2</sub>O<sub>2</sub> solution by different methods<sup>11-13</sup>. The investigation of the real-time dynamics of the modifications of cerium in terms of electronic properties and atomic environment during the dissociation of H<sub>2</sub>O<sub>2</sub>, would bring a valuable and reliable insight in the process. The design of an in-situ experiment is quite challenging, since it requires a liquid

<sup>a</sup> Dipartimento di Scienze Fisiche Informatiche e Matematiche, Università degli Studi di Modena e Reggio Emilia, Via G. Campi 213/a, 41125 Modena, Italy

<sup>b</sup> Consiglio Nazionale delle Ricerche, Istituto Nanoscienze, Via G. Campi 213/a, 41125 Modena, Italy

<sup>c</sup> European Synchrotron Radiation Facility, BP 220, 38043 Grenoble, France

<sup>d</sup> Department of Physics and Astronomy, University of Bologna, Viale C. Berti Pichat 6/2, 40127 Bologna, Italy

<sup>e</sup> Istituto Officina dei Materiali, Consiglio Nazionale delle Ricerche, Operative Group in Grenoble, c/o ESRF, BP 220, 38043 Grenoble, France

<sup>f</sup> Dipartimento di Scienze Chimiche e Geologiche, Università degli Studi di Modena e Reggio Emilia, Via G. Campi 183, 41125 Modena, Italy

Electronic Supplementary Information (ESI) available: [details of any supplementary information available should be included here]. See DOI: 10.1039/x0xx00000x

environment and an extremely high sensitivity due to the high dilution of the Ce species in the investigated samples.

High energy-resolution fluorescence detected X-ray absorption near-edge spectroscopy (HERFD-XANES) is a unique tool which combines the two requirements and it was already shown to be sensitive to very small modifications of the electronic structure of Ce ions<sup>15, 16</sup> also in liquid environment<sup>17</sup>. In this paper we report a Ce L<sub>3</sub>-edge HERFD-XANES study of Ce-doped bioactive glasses of different composition and morphology in situ and in real time during the reaction with aqueous solutions of H<sub>2</sub>O<sub>2</sub>. The results allow us to obtain valuable information on the active species and on the electronic mechanisms which come into play during the investigated reaction.

## Experimental methods and materials

Four different CeO<sub>2</sub>-modified bioactive glasses with different composition and morphology were investigated in the present study. Two of the glasses were synthesized using a melting procedure. The first was obtained by adding CeO<sub>2</sub> to 4555 Hench Bioglass®<sup>18</sup>, resulting in the following molar composition: SiO<sub>2</sub> 43.8 %, Na<sub>2</sub>O 23.0 %, CaO 25.5 %, P<sub>2</sub>O<sub>5</sub> 2.4 %, CeO<sub>2</sub> 5.3 %. This sample will be referred to as the H sample in the following. The second one was synthesized without phosphorous oxide, by adding CeO<sub>2</sub> to the glass introduced by Kim et al.<sup>19</sup> and resulted in the following molar composition: SiO<sub>2</sub> 48.2 %, Na<sub>2</sub>O 24.1 %, CaO 24.1 %, CeO<sub>2</sub> 3.6 %. This sample will be referred to as the K sample in the following. The synthesis of molten phosphorous-free glasses with CeO<sub>2</sub> concentration higher than 3.6% leads to a partial crystallization of the material. The details of the synthesis procedures for the H and K glasses can be found in references<sup>20</sup> and<sup>12</sup>, respectively. The specific surface area (SSA) of the samples obtained by melting after milling and sieving to 20-50 μm size is 1.5 m<sup>2</sup>/g for the H sample and 1.0 m<sup>2</sup>/g<sup>21</sup> for the K sample (see Supporting Information for details).

Two glasses with a mesoporous morphology were obtained by a sol-gel procedure coupled with evaporation-induced self-assembly (EISA) method as described in reference<sup>22</sup>. The molar composition of the glasses was SiO<sub>2</sub> 75.8 %, CaO 14.2 %, P<sub>2</sub>O<sub>5</sub> 4.7 %, CeO<sub>2</sub> 5.3 %. The obtained glasses have an average pore size of the order of a few nm and a SSA of 315 m<sup>2</sup>/g<sup>23</sup>. One of the two mesoporous glasses was treated at 700°C in oxygen atmosphere in order to obtain a larger fraction of cerium ions oxidized to the 4+ state. For this sample a SSA of 340 m<sup>2</sup>/g was measured (see Supporting Information). The two mesoporous samples will be referred to as MBG and MBG<sup>4+</sup> in the following.

In order to determine the surface charge of the materials during the experiments, we measured the pH value of points of zero charge (PZC). The method used is based on the determination of the intersection point of titration curves<sup>24</sup> (see also Supporting Information for more details). The obtained value (pH<sub>PZC</sub>) are 5.9 ± 0.2, 5.8 ± 0.1, 9.2 ± 0.4 and 9.1 ± 0.2 for MBG, MBG<sup>4+</sup>, H and K respectively.

The modifications of cerium ion oxidation state and local atomic environment in the samples during reaction with hydrogen peroxide solutions were investigated using HERFD-XANES. For these measurements a liquid-jet setup was used, as in reference<sup>17</sup>. The suspension of powdered glass (milled and sieved to achieve a grain size smaller than 100 μm) in water was continuously stirred and pumped through a closed circuit which takes it to the analysis region and back to the main container. The circuit includes a cut glass capillary tube, which allows the formation of a thin column of free liquid where the photon beam interacts with the sample. The setup allows to follow the modifications of the material during the reaction in real time, and to simultaneously minimize beam damage effects.

All the measurements were carried out first in ultra-pure water and then in a 0.1 M H<sub>2</sub>O<sub>2</sub> aqueous solution, except for a single run performed on MBG in a more concentrated 10 M H<sub>2</sub>O<sub>2</sub> solution. The glass concentration in the solution is 5 mg/ml for all samples, in analogy with our previous works<sup>11-14</sup>. The catalase mimetic activity of the four samples here investigated was assessed previously<sup>11-14</sup>. The H<sub>2</sub>O<sub>2</sub> dissociation as a function of time for each glass in 0.1 M H<sub>2</sub>O<sub>2</sub> aqueous solution is reported in Figure S1.

Two reference spectra were acquired to help the interpretation of the data measured on the glass samples. The reference for Ce<sup>3+</sup> was cerium nitrate hexahydrate (Ce(NO<sub>3</sub>)<sub>3</sub>·6H<sub>2</sub>O), while the reference for Ce<sup>4+</sup> was stoichiometric CeO<sub>2</sub>. Both reference samples in powdered form were mixed with cellulose and measured in the form of pellets, with a cerium oxide concentration comparable to the one of glass samples.

The HERFD-XANES measurements at the Ce L<sub>3</sub> edge were performed at the ID26 beamline of the European Synchrotron Radiation Facility<sup>25</sup>. The incident beam energy was selected with a Si(311) double crystal monochromator. Rejection of higher order harmonics is achieved by three Si mirrors working in total reflection conditions. The hard X-ray emission spectrometer was equipped with five spherically bent Ge(331) crystal analyzers and it was used for the detection of the Ce L<sub>1</sub> emission line (4839 eV). The total energy bandwidth was 0.5 eV. The spectra were acquired in the 5.714 - 5.800 keV energy range.

The acquisition time for individual HERFD-XANES spectra was approximately one minute, while the spectra here shown are averages over 20 spectra. Each sample was measured for times up to 140 min, except for the K sample, which was measured only for 80 min.

The spectra of the two reference samples and of the four glasses in pure water are shown in Figure 1. The data processing includes a normalization to the incident photon beam intensity and to the edge jump, modelled as an arctan function. **The fitting of the data using a linear combination of the spectra acquired on the two reference samples did not give satisfactory results, possibly because the local environments of the different Ce sites within the complex glass matrix are not equivalent to those in the reference oxide samples. To be able to identify the evolution of the fine**

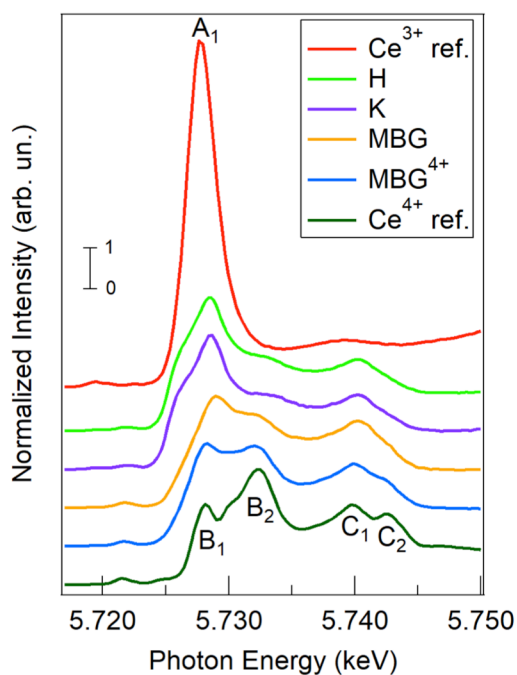


**Figure 1:** L<sub>3</sub>-edge HERFD-XANES spectra of Ce<sup>3+</sup> (red) and Ce<sup>4+</sup> (dark green) reference samples and of the H (green), K (purple), MBG (orange), and MBG<sup>4+</sup> (blue) glasses measured in pure water before the reaction.

structure of the spectra an empirical procedure was used for spectra fitting, which includes an arctan function for the atomic-like background, six gaussian peaks to account for the Ce<sup>4+</sup> related components and two gaussian peaks to account for the Ce<sup>3+</sup> related components (see Figure S2). The software used for data fitting was Fityk<sup>26</sup>. The first step of the fitting procedure consisted in fitting the spectrum of the sample with the highest Ce<sup>4+</sup> concentration, i.e. the spectrum of the MBG<sup>4+</sup> sample acquired after 140 min of reaction, with the nine fitting components, fixing the energy positions to the values obtained by fitting the Ce<sup>4+</sup> reference spectrum and using the intensities and the widths of the peaks as fitting parameters. This step was necessary since the width of the components in the amorphous samples here investigated was greater than the ones of the crystalline reference sample, as expected. After this step, the energy position and widths were fixed for each peak, while only the intensity was used as a free fitting variable for the various samples at the different reaction times. Since the energies of the A<sub>1</sub> and B<sub>1</sub> peaks are extremely close (Figure 1), only the A<sub>1</sub> component was used in the glass spectra fitting. The amplitude of the B<sub>1</sub> component was instead fixed to ratio  $B_1/(B_2+C_1+C_2)$  in the Ce<sup>4+</sup> reference, the amplitude of B<sub>2</sub>, C<sub>1</sub> and C<sub>2</sub> being fitting parameters. We emphasize here that the empirical fitting procedure used neglects the possible dependence of the position of the spectral features on the fine details of the local atomic environment of Ce. When cerium oxide is introduced in glasses as a low-concentration additive the average local atomic environment of Ce ions, and in particular its coordination and

distance to O ions, is indeed slightly modified compared to bulk oxide<sup>27</sup>. However, we believe that neglecting the influence of such small structural changes on the energy of spectral features may be a good approximation to follow as a function of time the fraction of Ce 3+ and 4+ ions in the different samples during the reaction. The absolute values of the oxidation state are however certainly affected by a large uncertainty, however all the consideration and conclusions of the present work are based on the variation of the oxidation state evaluated with the identified methodology, rather than on its absolute value. The existing calculations of Ce L<sub>3</sub> edge XANES spectra allow to identify the origin of each structure in bulk crystalline samples<sup>15, 28, 29</sup>, as reported below. The goodness-of-fit parameters  $\chi^2$  and R<sup>2</sup> for the different samples at different reaction times are reported in the Supporting Information (Table ST2 and ST3).

## Results

The Ce L<sub>3</sub>-edge HERFD-XANES spectra measured on the two reference samples and on the four glass samples before the reaction with H<sub>2</sub>O<sub>2</sub> are shown in Figure 1. The Ce<sup>3+</sup> reference shows a relatively simple spectrum, with a strong white line just above the absorption edge (labelled A<sub>1</sub>). The Ce<sup>4+</sup> reference exhibits a much more complex spectrum, dominated by two major features ascribed to screened and unscreened

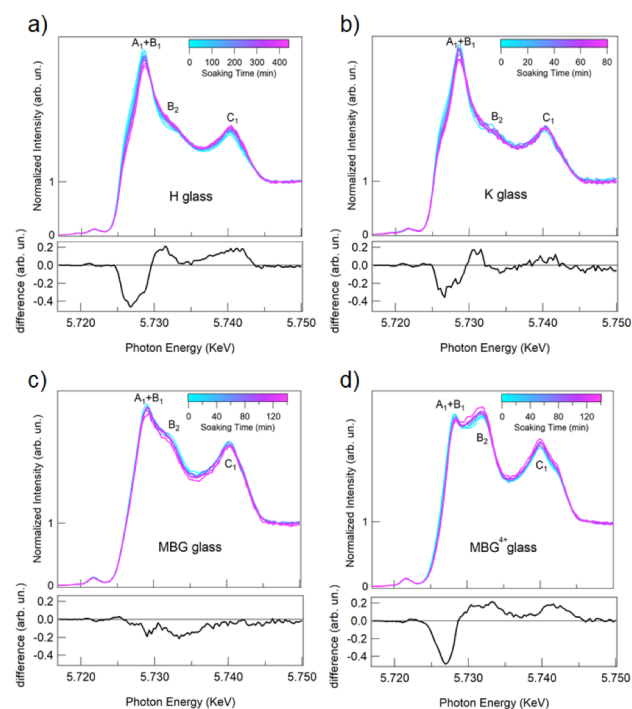


**Figure 2:** Evolution of the Ce L<sub>3</sub>-edge HERFD-XANES spectra during the reaction with a 0.1 M H<sub>2</sub>O<sub>2</sub> solution (top) and difference between the spectra acquired at the end and before the reaction (bottom) for (a) H, (b) K, (c) MBG, and (d) MBG<sup>4+</sup> glasses.

2p  $\rightarrow$  5d transitions (B and C peaks respectively, with an additional fine structure splitting ascribed to the crystal field, which gives origin to the two  $e_g$  and  $t_{2g}$  bands ( $B_1$ - $B_2$  and  $C_1$ - $C_2$ )<sup>15, 28, 29</sup>. The weak pre-edge features are linked to dipole forbidden 2p  $\rightarrow$  4f transitions, detectable only by HERFD-XANES. A clear energy difference can be detected between the absorption edge of the two references, as expected. The spectra of the H and K samples exhibit a similar shape, with a dominant peak energetically close to the  $Ce^{3+}$  white line (peak  $A_1$ ), although less intense and more structured than the reference spectrum, and two further features, close to peaks  $B_2$  and  $C_1$  of the  $Ce^{4+}$  reference spectrum. This indicates that cerium ions are present in the two oxidation states in the glass bulk, as previously observed by XPS on the glass surface<sup>11, 12</sup>. The spectrum of the MBG glass, on the contrary, shows a prevalence of peaks related to  $Ce^{4+}$  (peaks  $B_2$ ,  $C_1$  and  $C_2$ ) and a less pronounced  $A_1$  peak. The differences are even more evident on the post-annealed MBG<sup>4+</sup> spectrum. These qualitative observations, confirmed also by the shape of the pre-edge features shown in Figure S3, show that the mesoporous glasses contain a larger fraction of cerium ions in the 4+ state than glasses obtained by melting, confirming the differences observed on the surface by XPS<sup>11, 12, 14</sup>.

Figure 2 reports the spectra measured during the reaction with the 0.1 M  $H_2O_2$  water solution for the four samples. For the H, K and MBG<sup>4+</sup> samples (Figure 2 a, b and d) the reaction leads to a non-negligible evolution of the spectral shape towards a progressive oxidation with a decrease of the intensity of peak  $A_1$  and an increase of the intensity of peak  $B_2$  and  $C_1$ . This can be clearly seen also by inspecting the difference between the spectra acquired at the end and before the reaction, reported at the bottom of each panel in Figure 2. In the H, K and MBG<sup>4+</sup> samples a negative peak at 5.727 KeV indicates a shift of the edge jump to higher photon energies as the reaction proceeds. The two positive peaks correspond to increases in intensity at photon energies close to  $B_2$  and  $C_1$ . The evolution of the pre-edge spectral features for these three samples is also in agreement with a progressive oxidation, as shown in the Supporting Information in Figure S4. The MBG sample (Figure 2 c), shows a very small modification in the 0.1 M solution, despite the fact that, together with the MBG<sup>4+</sup>, it is the sample with the highest reactivity towards  $H_2O_2$  dissociation (see Figure S1). This sample was measured also during the reaction with a more concentrated 10 M solution. The spectra shown in Figure S5 Supporting Information show a marked oxidation of the sample in this case.

The results of the fitting of the spectra of the four samples using the procedure outlined in section 2 are summarized in Figure 3, which reports the ratio between the area of peak A, ascribed to  $Ce^{3+}$ , and the area of peaks B and C, ascribed to  $Ce^{4+}$ , for each sample as a function of reaction time in a 0.1 M  $H_2O_2$  solution and only for the MBG sample also in a 10 M solution. As already noticed by a qualitative analysis of the spectra, the initial  $Ce^{3+}$  concentration is larger in glasses obtained by melting (H and K samples) than in mesoporous ones. Moreover, in all samples the  $Ce^{3+}$  concentration decreases with reaction time. In the K sample the  $Ce^{3+}$

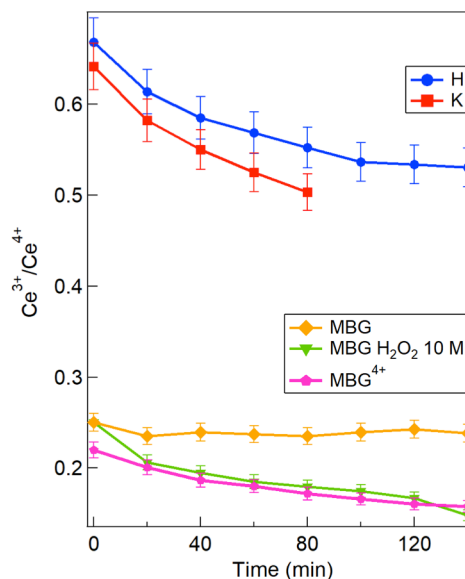


**Figure 3:** Evolution of the  $Ce^{3+}/Ce^{4+}$  ratio obtained by fitting of the HERFD-XANES spectra for the H, K, MBG, and MBG<sup>4+</sup> glasses during the reaction with a 0.1 M  $H_2O_2$  solution and for the MBG glass during reaction with a 10 M  $H_2O_2$  solution.

concentration undergoes a slightly faster decrease than in the H sample. The  $Ce^{3+}$  concentration in the MBG sample in 0.1 M solution shows no detectable changes for times up to 140 min, while in the 10 M solution it decreases significantly. The post-oxidized MBG<sup>4+</sup> sample shows an initially lower  $Ce^{3+}/Ce^{4+}$  ratio compared to the non-treated MBG sample and it undergoes a relevant oxidation.

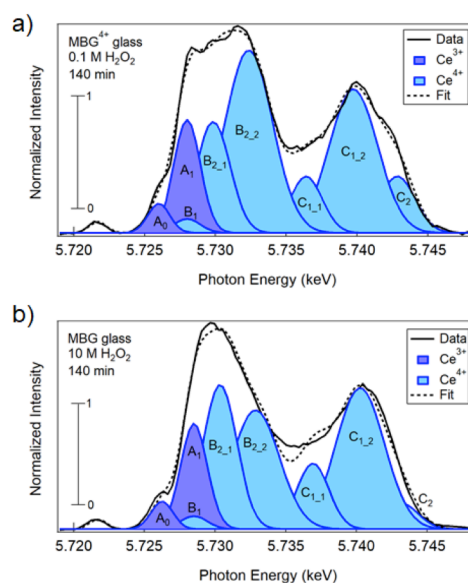


**Figure 4:** Ce  $L_3$ -edge HERFD-XANES spectra of MBG<sup>4+</sup> (a) and MBG (b) after 140 min in 0.1 and 10 M  $H_2O_2$ , respectively (dashed line). The individual fit components related to  $Ce^{3+}$  (blue) and to  $Ce^{4+}$  (light blue) and the overall fit (solid line) are also shown.

The MBG<sup>4+</sup> in 0.1 M H<sub>2</sub>O<sub>2</sub> solution and the MBG sample in 10 M H<sub>2</sub>O<sub>2</sub> solution have the same Ce<sup>3+</sup>/Ce<sup>4+</sup> ratio in the late stages of the reaction. Figure 4 reports the Ce L<sub>3</sub>-edge HERFD-XANES spectra of the two samples, together with the individual fit components and the overall fit of the spectrum. It is evident that the fine structure of the two spectra reported in Figure 4 is different. In the literature, modifications of the Ce L<sub>3</sub>-edge fine structure were observed in ceria nanoparticles of decreasing size and they were qualitatively ascribed to changes in Ce local environment and to spectral broadening due to higher disorder in smaller NPs<sup>17, 30</sup>. In particular, it is clear from Figure 4 that the relative intensity of peaks B<sub>2,1</sub> and B<sub>2,2</sub> in the two spectra is rather different. Also the relative intensity of the C features is not the same, although the B features are more intense and better reproduced by the fit. The evolution of the intensity ratio of peak B<sub>2,1</sub> and B<sub>2,2</sub> was analyzed for all samples investigated and it is reported in Figure 5. In all cases the ratio increases with reaction time. The H and MBG samples have an initial value of 0.48 and 0.52

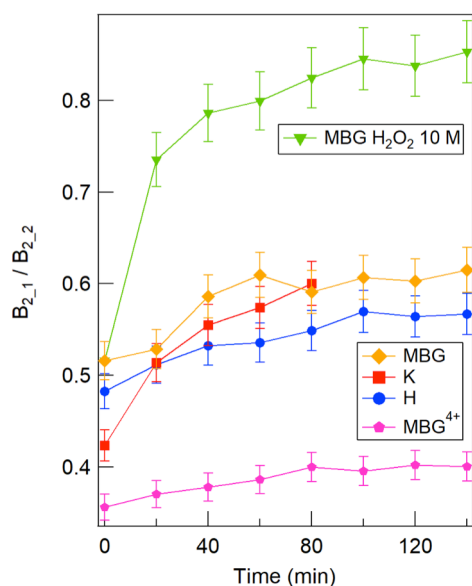


**Figure 5:** Evolution of the ratio of peak B<sub>2,1</sub> and B<sub>2,2</sub> in the fitting of the HERFD-XANES spectra for K, H, MBG and MBG<sup>4+</sup> during the reaction with a 0.1 M H<sub>2</sub>O<sub>2</sub> solution and for the MBG glass during reaction with a 10 M H<sub>2</sub>O<sub>2</sub> solution.

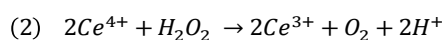
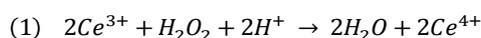
respectively, which increases with time by approximately 0.1. The K sample starts with an initially lower value of 0.42 and the increase is more pronounced than for the H and MBG samples. For the MBG sample in 10 M solution the B<sub>2,1</sub>/B<sub>2,2</sub> ratio increases very quickly in the first 20 min, assuming a value higher than 0.7, while the increase becomes progressively slower at longer times reaching 0.85 after 140 min. The MBG<sup>4+</sup> glass has a significantly lower B<sub>2,1</sub>/B<sub>2,2</sub> ratio compared to the other samples, below 0.4. The trends observed in Figure 5 will be discussed in the following section.

## Discussion

The analysis of the HERFD-XANES data before and during the reaction with H<sub>2</sub>O<sub>2</sub> allows to obtain very important information on the role of cerium ions in the catalase mimetic activity, which may be extended to Ce-containing materials in general.

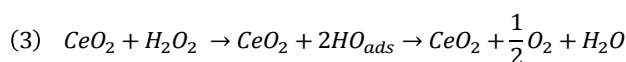
The mechanism which come into play in enzyme mimetic activity of cerium oxide have been under debate for years<sup>6, 7, 31-33</sup>. The reaction between H<sub>2</sub>O<sub>2</sub> and metal oxides may take place through a redox cycle<sup>34,5-7, 31, 35</sup> or through a non-redox mechanism<sup>36-38</sup>. Indeed several factors, like pH of the solution, stoichiometry and morphology of the oxide surface, defectivity, and temperature, have a strong effect on the kinetics and on the energetics of the reaction.

A widely accepted description of the redox cycle, introduced by Celardo et al.<sup>6</sup>, is given by the two reactions:



Indeed reaction (1) is favored in acid solutions while the reduction (2) is promoted in basic solutions<sup>33</sup>. We note also that the model requires the presence of oxygen vacancies both for reaction (1) and for reaction (2) to take place<sup>6</sup>.

The non-redox mechanism for decomposition of H<sub>2</sub>O<sub>2</sub> can be described by the following reaction<sup>38</sup>:



Typically, on cerium oxide the redox cycle dominates and a great number of studies show that cerium oxide acts as an enzyme mimetic material due to its redox properties<sup>5-7, 31, 35</sup>. The non-redox mechanism instead prevails at high temperatures in the vapour phase and in absence of H<sup>+</sup> ions<sup>37</sup>. The present work investigates the modifications of the Ce<sup>3+</sup>/Ce<sup>4+</sup> ratio in the samples during dissociation of H<sub>2</sub>O<sub>2</sub>, which take place during the redox cycle, but indeed also the possible non-redox mechanism has to be considered.

In our study we have investigated two classes of glasses: traditional glasses obtained by melting (H and K samples) and mesoporous glasses (MBG and MBG<sup>4+</sup> samples). The observed modifications of the oxidation state and local environment of Ce ions in the glasses during H<sub>2</sub>O<sub>2</sub> dissociation are discussed considering the differences in morphology, composition and local structure of Ce ions. At short reaction times, in the H<sub>2</sub>O<sub>2</sub> 0.1 M solution, the surfaces of the MBG and MBG<sup>4+</sup> glasses are negatively charged, having a lower pH<sub>PZC</sub> (5.9 and 5.8, respectively) with respect to the initial solution pH (6.3), while H and K are positively charged, having a higher pH<sub>PZC</sub> (9.1 and 9.2). The two glasses obtained by melting have a comparable pH<sub>PZC</sub> (9.1 and 9.2 for H and K respectively), and the same applies to the two mesoporous glasses (5.9 and 5.8 for MBG and MBG<sup>4+</sup> respectively). At long times the situation is more complex, since the solution pH gradually increases due the partial dissociation of H<sub>2</sub>O<sub>2</sub>, and by an ion exchange between

the  $\text{Ca}^{2+}/\text{Na}^+$  ions of the glasses and the  $\text{H}^+$  ions in the  $\text{H}_2\text{O}_2$  solution.

In general, we observed a decrease of the  $\text{Ce}^{3+}/\text{Ce}^{4+}$  ratio at short reaction times, which indicates that the redox reaction (1) dominates at short reaction times (Figure 3). At longer times, the  $\text{Ce}^{3+}/\text{Ce}^{4+}$  ratio tends to saturate, possibly due to the above mentioned increase of solution pH, which favors the reaction (2), leading to some balance between (1) and (2). Alternatively, the non-redox mechanism (reaction (3)) may dominate at longer times.

The relevantly higher SSA of mesoporous samples compared to traditional glasses indeed gives a first rationale for their higher activity for  $\text{H}_2\text{O}_2$  dissociation (Figure S1, Table ST1). Although the higher SSA of the MBG samples compared to H and K samples is the main cause for the different catalytic activity of the systems, also the glass composition may have a role. In a previous study Pirmohamed et al. correlated the catalase mimetic activity of cerium oxide nanoparticles with a low concentration of cerium in the 3+ oxidation state<sup>5</sup>. The lower initial  $\text{Ce}^{3+}/\text{Ce}^{4+}$  ratio of the mesoporous samples compared to H and K glasses (Figure 1 and 2) may therefore also be partly responsible for their higher activity (Figure S1). In sample K, which has a very similar initial  $\text{Ce}^{3+}$  concentration as H, the decrease of the  $\text{Ce}^{3+}$  concentration is slightly faster than for H (Figure 3), in agreement with the idea hypothesized in our previous studies<sup>12</sup> that the higher catalase mimetic activity, visible in Figure S1, is correlated with the absence of phosphorus, which stabilizes  $\text{Ce}^{3+}$  in H glasses. This hypothesis is corroborated also by the lower SSA measured on the K sample with respect to H sample (see table ST1), and it represents an important confirmation of the dependence of the activity of Ce not only on the initial concentration of  $\text{Ce}^{3+}$  ions, but rather on the actual reducibility of Ce ions which is determined by their local atomic environment.

On the contrary, the  $\text{Ce}^{3+}$  concentration does not change significantly in the MBG sample (Figure 3), which is the most reactive glass for  $\text{H}_2\text{O}_2$  dissociation (Figure S1). The rationale for this behavior may be the fact that the MBG sample has an optimal concentration of Ce ions in the two oxidation states for the two reactions (1) and (2) proceed with a comparable speed, without leading to detectable changes in the average concentration of the two ionic species. We note also that the  $\text{pH}_{\text{PZC}}$  for this sample (5.9) is much closer to the initial solution pH (6.3) than in molten samples. The different behavior of the  $\text{Ce}^{3+}/\text{Ce}^{4+}$  ratio in the MBG compared to the other samples demonstrates that their morphology, namely the SSA larger by a factor of approximately 300 in MBG glasses, is not the only factor which plays a role in the catalase-mimetic activity. Indeed, another possible explanation for the observed behavior could be the prevalence of the non-redox mechanism for  $\text{H}_2\text{O}_2$  dissociation (reaction 3) on this sample.

The decrease of  $\text{Ce}^{3+}$  concentration for the MBG sample in the 10 M  $\text{H}_2\text{O}_2$  solution can be explained by considering that in a more concentrated  $\text{H}_2\text{O}_2$  solution, with a lower pH (pH=5.3 for 10 M vs pH=6.3 for 0.1 M solution), the surface becomes negatively charged ( $\text{pH}_{\text{PZC}}$ =5.9) and the reaction (1) is expected to be faster.

A further confirm of the fact that not only SSA has a role in catalase mimetic activity of cerium oxide comes from the comparison of the dissociation of  $\text{H}_2\text{O}_2$  by the post-annealed  $\text{MBG}^{4+}$  sample (Figure S1), which is slower than the MBG sample in spite of its larger SSA (340  $\text{m}^2/\text{g}$ ), compared to MBG sample SSA (311  $\text{m}^2/\text{g}$ ). Moreover, the  $\text{MBG}^{4+}$  sample shows a non-negligible decrease of the  $\text{Ce}^{3+}/\text{Ce}^{4+}$  ratio during the reaction in spite of the initially lower ratio compared to the MBG one (Figure 3), which indicates that reaction (1) dominates over reaction (2). Being the measured  $\text{pH}_{\text{PZC}}$  comparable in the MBG and  $\text{MBG}^{4+}$  samples (5.9 and 5.8 respectively), we consider the presence of Ce ions with different local environments and the different mechanisms which oxidize/reduce Ce ions to explain the observed decrease of the  $\text{Ce}^{3+}/\text{Ce}^{4+}$  ratio. Celardo et al.<sup>6</sup> introduced the idea that the active sites for  $\text{H}_2\text{O}_2$  dissociation through reaction (2) are  $\text{Ce}^{4+}$  ions in proximity of an O vacancy. In spite of the higher complexity of the system here investigated and of the different average local atomic environment of Ce ions in glasses than in oxides<sup>27</sup>, it is reasonable to assume that the post-oxidation treatment in oxygen undergone by the  $\text{MBG}^{4+}$  glass results in a filling of part of the oxygen vacancies present in the material. Part of the  $\text{Ce}^{3+}$  sites will be transformed into  $\text{Ce}^{4+}$  sites fully coordinated by oxygen ions, for which the activation energy to contribute to the reaction by the formation of an oxygen vacancy would be too high (its value is around 2 eV on extended cerium oxide surfaces<sup>39</sup>). For this reason, in the  $\text{MBG}^{4+}$  sample, even if the initial  $\text{Ce}^{3+}$  concentration is lower than in the MBG sample, the catalase mimetic activity is comparable (Figure S1) and reaction (1) dominates inducing a further decrease in  $\text{Ce}^{3+}$  concentration (Figure 3). The existence of  $\text{Ce}^{4+}$  sites with different local environments in MBG and  $\text{MBG}^{4+}$  samples can therefore explain the observed trend for the corresponding  $\text{Ce}^{3+}/\text{Ce}^{4+}$  ratio in Figure 3.

In a previous x-ray photoelectron spectroscopy (XPS) study of the Ce average surface oxidation state in H samples measured ex-situ after soaking for different times in 0.1 M  $\text{H}_2\text{O}_2$ , we observed a similar decreasing trend of the surface  $\text{Ce}^{3+}$  concentration after short reaction times<sup>11</sup>. Expectedly the decrease detected by a surface sensitive technique such as XPS appears faster compared to the one measured by XANES which probes the whole sample thickness. On the other hand, in our previous XPS study the surface Ce oxidation state composition was possibly partially altered by air exposure after each reaction step. The present study in which the XANES are acquired in-situ during the reaction, gives a reliable evidence for a net increase of the average Ce oxidation state while mimicking the catalase enzyme functionality. Longer reaction times (> 4h), which were observed by XPS to induce a partial reduction of the surface Ce ions<sup>11</sup>, could not be accessed by the present investigation.

It has also to be noted that, besides the modifications of the concentration of the two Ce ionic species, also modifications of the Ce  $L_3$ -edge lineshape during the reaction could be detected by the high-resolution method here used. The spectral modifications induced by  $\text{H}_2\text{O}_2$  dissociation were analyzed by comparing the intensity ratio of the peaks used for the fitting.

We have chosen the ratio between  $B_{2,1}$  and  $B_{2,2}$  peaks, both peaks related to the  $t_{2g}$  band, as representative of the modifications observed (Figure 5). As previously discussed two different kinds of  $Ce^{4+}$  sites may be present in the glass samples: non active  $Ce^{4+}$  sites with high coordination of oxygen ions and  $Ce^{4+}$  ions in proximity of oxygen vacancies active for the catalase mimetic activity. The  $B_{2,1}$  and  $B_{2,2}$  peak positions and relative intensities are expected to be influenced by the arrangement of O ions around the Ce ion. For all samples the  $B_{2,1} / B_{2,2}$  ratio increases as the reaction with  $H_2O_2$  proceeds, in other words the reaction induces the formation of Ce species with a dominant  $Ce^{4+}$ -related  $B_{2,1}$  component. Even in the MBG sample, in which the  $Ce^{3+}/Ce^{4+}$  ratio does not change, a non-negligible increase in the  $B_{2,1} / B_{2,2}$  ratio is observed as the reaction proceeds. Moreover, the marked increase of the ratio in the MBG sample in 10 M solution and the very evident differences in spectral shapes of two samples with a comparable average oxidation state – namely the MBG sample in 10 M solution and MBG<sup>4+</sup> sample in 0.1 M solution after 140 min of reaction (Figure 4) – further confirm that  $H_2O_2$  dissociation actually induces the formation of Ce species with a dominant  $B_{2,1}$  component. Also the faster increase of the  $B_{2,1} / B_{2,2}$  ratio for the K sample compared to the H sample is consistent with this picture, and it can be explained by the higher concentration of  $Ce^{3+}$  ions which can be transformed into  $Ce^{4+}$  sites with a neighbouring O vacancy, due to the absence of P ions which stabilize a fraction of the  $Ce^{3+}$  in the H sample. A further confirmation of the assignment of the  $B_{2,2}$  peak as dominant in samples containing fully coordinated  $Ce^{4+}$  ions and of  $B_{2,1}$  as dominant for  $Ce^{4+}$  ions with lower coordination of oxygen comes from the significantly lower initial  $B_{2,1} / B_{2,2}$  ratio in the MBG<sup>4+</sup> sample, in which the oxygen thermal treatment has very likely filled part of the oxygen vacancies. We therefore identify the  $B_{2,1}$  component as the spectroscopic signature of the  $Ce^{4+}$  phase which is active for the catalase mimetic activity. Indeed, some minor crystal-field related modifications are expected also for the components of the C peak, although their lower intensity in the spectra makes their identification more difficult than for the B peak.

## Conclusions

By HERFD-XANES at the Ce  $L_3$  edge we investigated the real-time evolution of the oxidation state and of the local atomic environment of cerium ions used as additive in bioactive glasses during the reaction with a solution of water and hydrogen peroxide. In glasses obtained by traditional melting the  $Ce^{3+}/Ce^{4+}$  ratio shows a significant decrease during reaction with  $H_2O_2$ . The decrease is slightly faster in phosphorous free glasses, possibly because the Ce ions are not stabilized in the 3+ state by phosphorous. In mesoporous samples with a significantly higher **specific surface area** the  $Ce^{3+}/Ce^{4+}$  trend is shown to depend not only on the initial concentration of the two ionic species in the samples but also on the local atomic environment of  $Ce^{4+}$  ions. The tendency for the concentration of the two Ce ionic species to reach an

equilibrium at long reaction times is discussed considering the variations of pH in the solutions close to the surface and the consequent equilibrium between reduction and oxidation. The catalase mimetic activity is indeed much higher in samples with higher **specific surface area**. In samples with comparable **specific surface area** we show that the higher reactivity correlates with a higher concentration of  $Ce^{4+}$  ions. The high resolution of the technique allowed to observe a modification in the  $Ce^{4+}$ -related spectral features, which provides a spectroscopic signature for the  $Ce^{4+}$  sites which are active for the catalase mimetic activity.

## Conflicts of interest

There are no conflicts of interest to declare.

## Acknowledgements

The authors wish to thank the European Synchrotron Radiation Facility for provision of beamtime and the staff of the ID26 beamline for excellent support during the setup of the experiment. Pieter Glatzel is gratefully acknowledged for stimulating discussions and for a critical reading of the manuscript.

## Notes and references

1. B. Halliwell, M. V. Clement and L. H. Long, *FEBS Letters*, 2000, **486**, 10-13.
2. F. L. Muller, M. S. Lustgarten, Y. Jang, A. Richardson and H. Van Remmen, *Free Radical Biology and Medicine*, 2007, **43**, 477-503.
3. E. Cadenas and K. J. A. Davies, *Free Radical Biology and Medicine*, 2000, **29**, 222-230.
4. W. Dröge, *Physiological Reviews*, 2002, **82**, 47-95.
5. T. Pirmohamed, J. M. Dowding, S. Singh, B. Wasserman, E. Heckert, A. S. Karakoti, J. E. S. King, S. Seal and W. T. Self, *Chemical Communications*, 2010, **46**, 2736-2738.
6. I. Celardo, J. Z. Pedersen, E. Traversa and L. Ghibelli, *Nanoscale*, 2011, **3**, 1411-1420.
7. E. G. Heckert, A. S. Karakoti, S. Seal and W. T. Self, *Biomaterials*, 2008, **29**, 2705-2709.
8. P.-A. Mouthuy, S. J. B. Snelling, S. G. Dakin, L. Milković, A. Č. Gašparović, A. J. Carr and N. Žarković, *Biomaterials*, 2016, **109**, 55-68.
9. L. L. Hench, *Journal of the American Ceramic Society*, 1991, **74**, 1487-1510.
10. A. J. Salinas and M. Vallet-Regi, *RSC Advances*, 2013, **3**, 11116-11131.
11. V. Nicolini, E. Gambuzzi, G. Malavasi, L. Menabue, M. C. Menziani, G. Lusvardi, A. Pedone, F. Benedetti, P. Luches, S. D'Addato and S. Valeri, *J Phys Chem B*, 2015, **119**, 4009-4019.
12. V. Nicolini, E. Varini, G. Malavasi, L. Menabue, M. C. Menziani, G. Lusvardi, A. Pedone, F. Benedetti and P. Luches, *Materials & Design*, 2016, **97**, 73-85.

13. V. Nicolini, G. Malavasi, L. Menabue, G. Lusvardi, F. Benedetti, S. Valeri and P. Luches, *Journal of Materials Science*, 2017, DOI: 10.1007/s10853-017-0867-2, 1-13.
14. G. M. Valentina Nicolini, Ledi Menabue, Gigliola Lusvardi, Francesco Benedetti, Giuseppina Cerrato, Sergio Valeri, Paola Luches, *in preparation*, 2018.
15. K. O. Kvashnina, S. M. Butorin and P. Glatzel, *Journal of Analytical Atomic Spectrometry*, 2011, **26**, 1265-1272.
16. G. Gasperi, L. Amidani, F. Benedetti, F. Boscherini, P. Glatzel, S. Valeri and P. Luches, *Phys Chem Chem Phys*, 2016, **18**, 20511.
17. J. D. Cafun, K. O. Kvashnina, E. Casals, V. F. Puentes and P. Glatzel, *Acs Nano*, 2013, **7**, 10726-10732.
18. L. L. Hench, *Journal of the American Ceramic Society*, 1998, **81**, 1705-1728.
19. H.-M. Kim, F. Miyaji, T. Kokubo, C. Ohtsuki and T. Nakamura, *Journal of the American Ceramic Society*, 1995, **78**, 2405-2411.
20. C. Leonelli, G. Lusvardi, G. Malavasi, L. Menabue and M. Tonelli, *J Non-Cryst Solids*, 2003, **316**, 198-216.
21. G. Lusvardi, G. Malavasi, L. Menabue, V. Aina and C. Morterra, *Acta Biomaterialia*, 2009, **5**, 3548-3562.
22. A. López-Noriega, D. Arcos, I. Izquierdo-Barba, Y. Sakamoto, O. Terasaki and M. Vallet-Regí, *Chemistry of Materials*, 2006, **18**, 3137-3144.
23. A. J. Salinas, S. Shruti, G. Malavasi, L. Menabue and M. Vallet-Regí, *Acta Biomaterialia*, 2011, **7**, 3452-3458.
24. K. Bourikas, C. Kordulis and A. Lycourghiotis, *Environmental Science & Technology*, 2005, **39**, 4100-4108.
25. C. Gauthier, V. A. Solé, R. Signorato, J. Goulon and E. Moguiline, *Journal of Synchrotron Radiation*, 1999, **6**, 164-166.
26. M. Wojdyr, *Journal of Applied Crystallography*, 2010, **43**, 1126-1128.
27. F. Benedetti, P. Luches, S. D'Addato, S. Valeri, V. Nicolini, A. Pedone, M. C. Menziani and G. Malavasi, *Journal of the American Ceramic Society*, 2017, **100**, 5086-5095.
28. A. Bianconi, A. Marcelli, H. Dexpert, R. Karnatak, A. Kotani, T. Jo and J. Petiau, *Phys Rev B*, 1987, **35**, 806-812.
29. A. V. Soldatov, T. S. Ivanchenko, S. Della Longa, A. Kotani, Y. Iwamoto and A. Bianconi, *Phys Rev B*, 1994, **50**, 5074-5080.
30. C. Paun, O. V. Safonova, J. Szlachetko, P. M. Abdala, M. Nachtegaal, J. Sa, E. Kleymenov, A. Cervellino, F. Krumeich and J. A. van Bokhoven, *The Journal of Physical Chemistry C*, 2012, **116**, 7312-7317.
31. A. Karakoti, S. Singh, J. M. Dowding, S. Seal and W. T. Self, *Chemical Society Reviews*, 2010, **39**, 4422-4432.
32. P. B. Sigler and B. J. Masters, *J Am Chem Soc*, 1957, **79**, 6353-6357.
33. T. J. Sworski, H. A. Mahlman and R. W. Matthews, *The Journal of Physical Chemistry*, 1971, **75**, 250-255.
34. F. W. J. Haber, *Proceedings of the Royal Society of London. Series A - Mathematical and Physical Sciences*, 1934, **147**, 332.
35. H. Wei and E. Wang, *Chemical Society Reviews*, 2013, **42**, 6060-6093.
36. E. B. Spear, *J Am Chem Soc*, 1908, **30**, 195-209.
37. A. Hiroki and J. A. LaVerne, *The Journal of Physical Chemistry B*, 2005, **109**, 3364-3370.
38. C. M. Lousada, M. Yang, K. Nilsson and M. Jonsson, *Journal of Molecular Catalysis A: Chemical*, 2013, **379**, 178-184.
39. M. Nolan, J. E. Fearon and G. W. Watson, *Solid State Ionics*, 2006, **177**, 3069-3074.